Cellulose (2019) 26:1209–1219
https://doi.org/10.1007/s10570-018-2124-5

ORIGINAL PAPER

Selective extraction of gadolinium using free-standing imprinted mesoporous carboxymethyl chitosan films with high capacity

Xudong Zheng · Yi Zhang · Tingting Bian · Yuzhe Zhang · Fusheng Zhang · Yongsheng Yan

Received: 12 July 2018 / Accepted: 7 November 2018 / Published online: 11 November 2018

Abstract Novel imprinted mesoporous carboxymethyl chitosan films (IMCFs) were investigated in detail. When acting as adsorbents, imprinted mesoporous carboxymethyl chitosan films with highly ordered chiral nematic structures, exhibit efficient adsorption for gadolinium ions (Gd(III)). The maximum adsorption capacity of IMCFs calculated from Langmuir isotherm model was 25.372 mg g^{-1} at pH 7.0. Due to the presence of highly selective imprinted sites, chitosan films possess significant selectivity for Gd(III), compared with other rare earth ions. More importantly, carboxymethyl chitosan films could be retrieved conveniently and quickly without extra operations, which greatly promote their recycling. Reusability tests further demonstrated films can be considered as stable and reliable adsorbents, enhancing their potential industrial applications.

Electronic supplementary material The online version of this article (https://doi.org/10.1007/s10570-018-2124-5) contains supplementary material, which is available to authorized users.

X. Zheng · Y. Zhang · T. Bian · Y. Zhang
School of Environmental and Safety Engineering, Changzhou University, Changzhou 213164, People's Republic of China

F. Zhang · Y. Yan (✉)
School of Chemistry and Chemical Engineering, Jiangsu University, Zhenjiang 212013, People's Republic of China
e-mail: yanys1@outlook.com

Graphical abstract

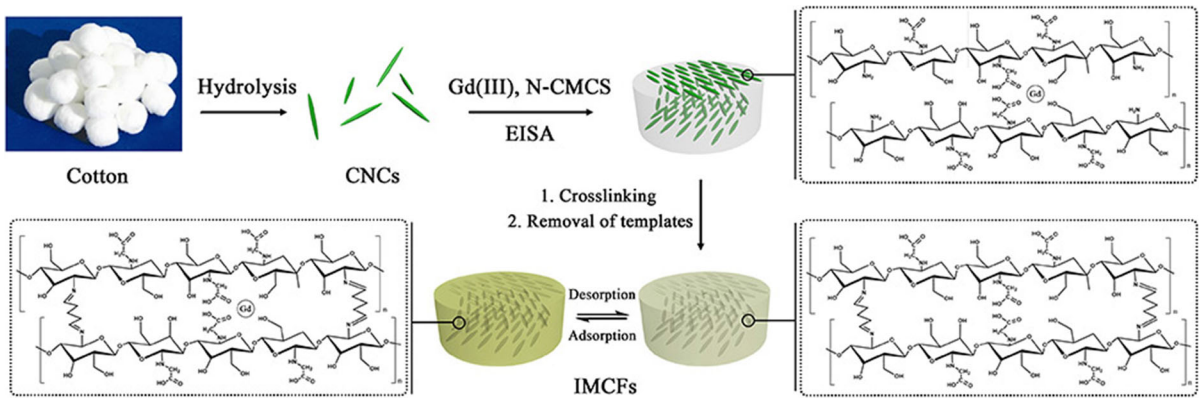

Keywords Solid–liquid extraction · Dysprosium · Ion imprinting · Mesoporous chitosan films

Introduction

Rare earth elements (REEs), owing to their unique physicochemical properties, are of high importance in the green technologies, such as hybrid electric vehicles, wind turbines, fuel cells and photovoltaics (Rollat et al. 2016). Chinese rare earth production once supplied more than 90% of the world. In 2011, China began to limit rare earth exports. Crisis in supply and rapid demand growth of REEs resulted in skyrocketing prices of REEs in just a few years (Ayora et al. 2016; Cho 2013; Woodcock and Hayward 2016). Among REEs, gadolinium (Gd) is recognized as one of the most crucial REEs because of its scarcity and critical value (Pavel et al. 2017). The chemical similarities of rare earth elements make it difficult to separate them from each other by physical or chemical methods. Hence, development of an effective and selective separation strategy for the separation of REEs is essential.

Commercial separations of REEs mainly include hydrometallurgy and pyrometallurgy. Hydrometallurgy requires multiple sequential extraction steps, which need large volume of hazardous solvents and generate significant amounts of undesired wastes (Larsson and Binnemans 2014). Compared with the hydrometallurgical route, fewer steps are needed for pyrometallurgy method, but it requires larger energy input, which imposes a burden on the environment (Kim et al. 2015). Solid–liquid extraction is a simpler and greener alternative due to its simplicity, flexibility, cost effectiveness, high efficiency, and less consumption of dangerous reagents (Wang et al. 2016; Yao et al. 2017). Over recent decades, variety of adsorbent materials have been developed for REE separation (Smith et al. 2016; Zheng et al. 2014). However, adsorbents with specific recognition capability are rarely reported.

Ionic imprinted polymers (IIPs) have received widespread attention with advantages of cost-effective, efficient, and selective adsorption with template ionic imprinted sites, which are regarded as promising candidates for adsorption of REEs (Bahrami et al. 2015; Gao et al. 2014; Xu et al. 2016). Chitosan (CS), rich in functional groups (–NH_2 and –OH), easiness in being cross-linked with dialdehydes, such as glutaraldehyde (He and Chen 2014). Recently, IIPs based on CS were studied for adsorption of metal ions (Fu et al. 2015; He et al. 2015; Kyzas et al. 2015). However, almost all investigated CS-based IIPs were made into powdered submicron beads, which led template ions are difficult to be removed completely due to embedding. In order to improve this defect, our previous studies designed three-dimensionally interconnected macroporous imprinted chitosan films to adsorb and separate Nd(III) (Zheng et al. 2016c). Our imprinted chitosan films exhibited accessibility to imprinted sites and selectivity. But, there are still several snags for CS-based IIPs materials: (1) preparation of colloidal crystal templates is difficult and time-consuming. (2) selectivity of CS-based IIPs, which is not the rigid structure, often decreases by use of the repetition.

Surfactant molecules or lyotropic liquid crystals, employed as templates for mesoporous materials, can be traced back 20 years (Guan et al. 2012; Luo et al. 2016; Ma et al. 2012). The hard or soft templates employed generally provide different mesoporous structures. As an extension of this method, biological materials, such as cellulosic derivatives, are typical hard templates with the ability to form chiral liquid crystalline phase. Thomas reported chiral nematic silica/hydroxy-propylcellulose (HPC) monoliths, while HPC plays the role of template (Thomas and Antonietti 2003). Cellulose nanocrystals (CNCs) prepared by acid-catalyzed hydrolysis of bulk cellulose, is regarded as cheap and environmental friendly template for porous materials. Dujardin prepared CNC/silica composites using CNCs as template. Although pore structure of material exhibits some nematic order, long-range chiral ordering cannot be observed clearly (Dujardin et al. 2003). Previously, it has been reported new type of mesoporous films templated with cellulose nanocrystallines (CNCs) (Qi et al. 2011; Shopsowitz et al. 2012). The resulting film materials have chiral nematic mesoporous organization just by evaporation-induced self-assembly (EISA). Consequently, these films process high specific surface, which can be applied in hosts for new nanostructured materials and chromatographic separation.

Pristine chitosan only dissolves in acid solution, which limits its application. Carboxymethyl chitosan (CMC), one of critical derivatives of water-soluble chitosan, possesses multiple functional groups on its surface, which may significantly increase adsorption capacity based on Hard–Soft Acid–Base theory (HSAB theory).

Herein, we prepared free-standing imprinted mesoporous carboxymethyl chitosan films (IMCFs) templated by CNCs. These films have high specific surface and selectivity for adsorption of Gd(III). The morphology of IMCFs was performed by TEM and SEM. Batch adsorption experiments of IMCFs were investigated for feasibility of REEs recovery, compared with non-imprinted carboxymethyl chitosan films (NIMCFs). The influence of operational parameters (pH, temperature) on the adsorption property was investigated systematically. In addition, reusability tests of IMCFs were also conducted and discussed in detail. High adsorption capacity, selectivity and simple retrieved without additional operations, making these novel imprinted films economically feasible for adsorption of Gd(III).

Experimental section

Preparation of materials

All reagents and solvents were purchased from Sinopharm Chemical Reagent Co. Ltd, in accordance with the analytical standards and used without further purification.

Preparation of cellulose nanocrystalline (CNCs)

Based on our previously reported (Zheng et al. 2016b). In brief, milled cotton was catalyzed hydrolysis with sulphuric acid for 2 h at 45 °C. Then, the mixture was diluted with 8-10 times cold deionized water to terminate hydrolysis reaction. After supernatant was discard, the remaining turbid layer was rinsed three times with deionized water to remove all soluble cellulosic materials, and then placed inside dialysis membrane tube for 1–4 days until the pH was about 2.4. Before each use, 10 min of sonication is required to disperse the solution evenly.

Preparation of free-standing imprinted mesoporous carboxymethyl chitosan films (IMCFs)

7.5 mg of $Gd(NO_3)_3$ $6H_2O$ and 20 mg of carboxymethyl chitosan were first dissolved in 5 mL of deionized water, and stirred for 2 h to form a Gd(III) complex. Subsequently, 5 mL of 6 wt% CNCs suspension and 0.40 mL tetramethoxysilane (TEOS) were added into solution. The homogeneous mixture was obtained by stirring at 60 °C for 4.0 h, and then poured into a polystyrene Petri dish (d = 7 cm). CNCs/carboxymethyl chitosan composite films were obtained after solution evaporation. These composite films were immersed in 3% of glutaraldehyde to crosslink with Gd(III)-carboxymethyl chitosan. Then films were placed into 1 L of 4 M sulfuric acid and heated in an orbital shaker to 70–80 °C. Free-standing imprinted mesoporous carboxymethyl chitosan films (IMCFs) were obtained by fetched and washed with deionized water for three times. The synthesis of non-imprinted mesoporous carboxymethyl chitosan films

(NIMCFs) is identical to that of IMCFs except no Gd(III) were added.

Instrument

The surface morphology of IMCFs and NIMCFs was observed by scanning electron microscope JSM-7001F. The internal pore structure of adsorbents was obtained by transmission electron microscopy JEM-2100. Nitrogen adsorption–desorption isotherms of the films were measured by Micromeritics TriStar II 3020 analyzer. Prior to nitrogen adsorption analysis, IMCFs and NIMCFs were degassed at 80 °C for 12 h and adsorption process was carried out at − 196° C. Surface groups of film materials were detected by Nicolet NEXUS-470 FT-IR apparatus. Elemental analysis was performed by the combustion method using CHNS Analyzer Flash 1112A, Thermo Scientific.

Batch adsorption experiments

The adsorption capacity $Q_{t(e)}$ (mg g^{-1}) of Gd(III) was calculated according to Eq. (1).

$$Q_t = \frac{V\left(C_o - C_{t(e)}\right)}{M} \quad (1)$$

where C_0 (mg L^{-1}) and $C_{t(e)}$ (mg L^{-1}) are the initial and residual concentration of Gd(III) after time t (or equilibrium), respectively. M (10 mg) and V (10 mL) indicate the mass of materials and volume of the stock solution, respectively.

Effect of pH

10 mg of IMCFs and NIMCFs were mixed with 10 mL of Gd(III) stock solution (50 mg L^{-1}, 298 K) under different pH value (1.0–7.0). When adsorption reached equilibrium, IMCFs and NIMCFs were fetched and the residual Gd(III) concentration in solution was determined by ICP-OES and repeated three times.

Kinetic studies

10 mg of IMCFs and NIMCFs were mixed with 10 mL of Gd(III) stock solution (50 mg L^{-1}, pH = 7). Concentration of Gd(III) was determined by ICP-OES at different contact time until saturated adsorption was reached and whole experiments were repeated three times.

Effect of temperature

10 mg of IMCFs and NIMCFs were mixed with 10 mL of Gd(III) stock solution (50 mg L^{-1}, pH = 7) at different temperatures (298 K, 308 K and 318 K). Concentration of Gd(III) was determined by ICP-OES and repeated three times.

Isotherm studies

10 mg of IMCFs and NIMCFs were mixed with 10 mL of a range of concentrations of Gd(III) stock solution (pH = 7.0). Residual Gd(III) concentration in solution was determined by ICP-OES and repeated three times.

Selectivity studies

Selectivity of IMCFs and NIMCFs were evaluated through competitive adsorption experiments. The stock solution (pH = 7.0, 298 K) was prepared by a mixed solution of Gd(III), Dy(III), Tb(III), Pr(III) and Nd(III), and concentration of each cation is 50 mg L^{-1}. 10 mg of IMCFs and NIMCFs were mixed with 10 mL of the stock solution. Residual concentration of each cation was determined by ICP-OES.

Reusability studies

After the adsorption, IMCFs were removed from the solution and rinsed several times with distilled water. HAc was applied to regenerate films. The entire adsorption–desorption cycle was repeated 5 times.

Results and discussion

Characterization of the materials

The chiral nematic mesoporous organization of IMCFs and NIMCFs was confirmed by SEM from the cross-sectional section of films. A periodic chiral nematic mesoporous structure of IMCFs is clearly observed (Fig. 1a). Mesoporous carboxymethyl chitosan films were also obtained without silica

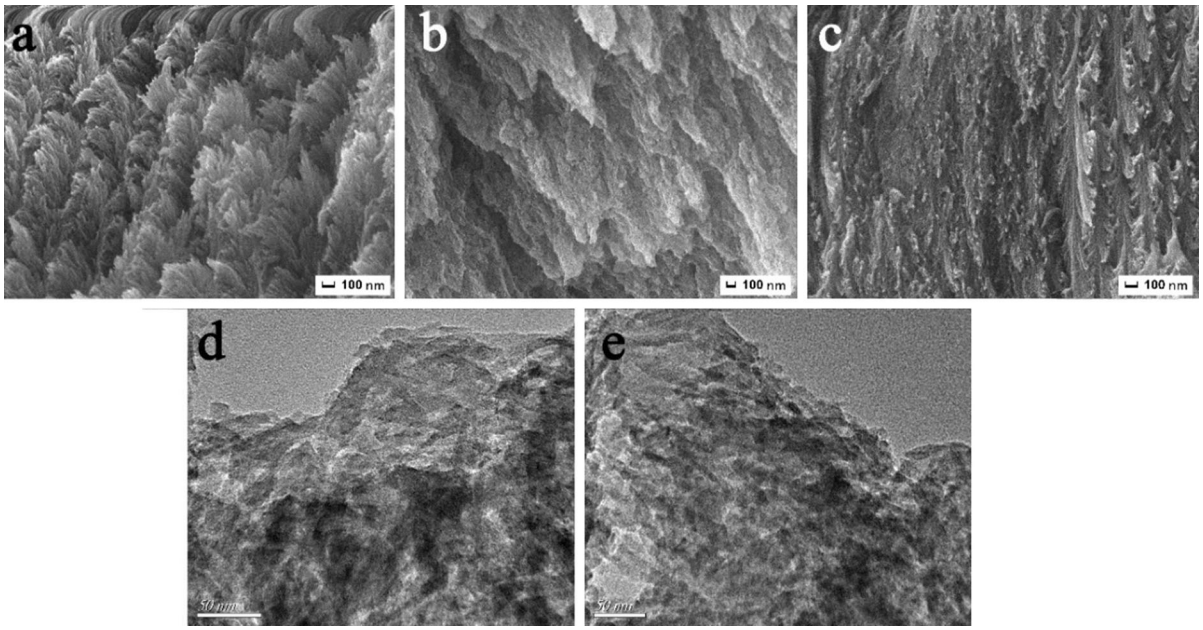

Fig. 1 SEM images of **a** IMCFs, **b** IMCFs without TEOS, **c** NIMCFs and TEM images of **d** IMCFs, **e** NIMCFs

Table 1 Brunauer–Emmet–Teller surface areas (S_{BET}) obtained by N_2 adsorption–desorption measurements for NIMCFs and IMCFs

Materials	S_{BET} (m^2 g^{-1})	Pore size (nm)	V_{proe} (cm^3 g^{-1})
NIMCFs	256.93	6.3167	0.4792
IMCFs	362.13	6.0335	0.4953

incorporation (Fig. 1b). Without silica support, chitosan films could not maintain excellent mesoporous structure. A similar mesoporous structure with IMCFs can be also observed in NIMCFs (Fig. 1c). From the figure, films cannot remain mesoporous organization owing to CMCs shrinkage and deformation. Therefore, adding silica significantly improved the mechanical stability of the film matrix. TEM images (Fig. 1d, e) of IMCFs and NIMCFs both show long spindle-shaped pores in arrays, which is close to the fusiform CNCs template.

Fig. S1 Shows N_2 adsorption–desorption isotherms for IMCFs and NIMCFs, both of them exhibit typical type IV isotherms with a distinctive H1 hysteresis loop. Corresponding test results were summarized in Table 1. As is shown, S_{BET} values of IMCFs and NIMCFs are about 362.13 m^2 g^{-1} and 256.93 m^2 g^{-1}, respectively. In the preparation of IMCFs, the incorporation of metal template ions brings stable imprinting sites on the surface of IMCFs, which may result in the surface area of IMCFs is much larger than that of NIMCFs.

The FT-IR spectra of IMCFs and NIMCFs demonstrate no significant differences (Fig. S2). However, adsorption peaks of carboxymethyl chitosan of all the samples are distinctive. The infrared spectra of IMCFs and NIMCFs shows a wide absorption band appeared at 3430 cm^{-1} corresponding to the stretching vibration of -NH_2 group and -OH group. Due to steric effect resulting from the introduction of glutaraldehyde, the absorb band at 1629 cm^{-1} and 1067 cm^{-1} assign to the stretching vibration of C=O of $–COO^-$ group and vibration of the secondary C–OH, respectively. The element analysis was also performed on IMCFs and NIMCFs, and each component of C, H and N was listed in Table 2. For both of IMCFs and NIMCFs, results seem to be similar.

The effect of pH

pH value is a critical factor restricting adsorption experiments. Rare earth ions may form insoluble precipitate in basic solutions. Figure 2 shows adsorption capacities of IMCFs and NIMCFs under different pH value (2.0–7.0). Adsorption capacities of IMCFs

Table 2 Elemental composition of materials from elemental analysis

Materials	N (%)	C (%)	H (%)
NIMCFs	0.797	27.295	4.533
IMCFs	0.636	30.032	4.840

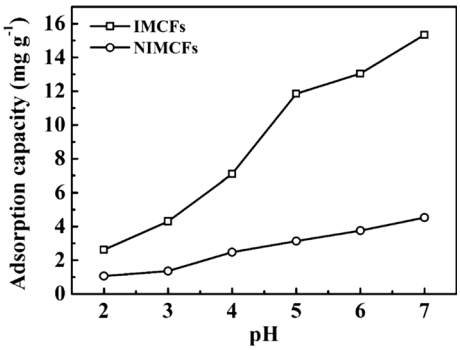

Fig. 2 The effect of pH on the adsorption capacity of IMCFs and NIMCFs

and NIMCFs raise with increasing pH value. The adsorption was performed by interactions between Gd(III), carboxyle groups (–COO^-) and amino groups (–NH_2) of CMCs. With increasing value of pH, –COO^- and –NH_2 groups provide a better adsorption effect, then adsorption capacity enhances. The adsorption capacity of IMCFs is much stronger than that of NIMCFs. It is attributable to that more imprinted cavities are immobilized on the surface of IMCFs compared with NIMCFs. In low pH conditions, reduced binding ability of Gd(III) may attribute to the protonation of amino groups. Therefore, the initial pH value of subsequent experiments was chosen as 7.0.

Adsorption kinetics

Figure 3 shows adsorption kinetic cures of IMCFs and NIMCFs. Pseudo-first-order kinetic model (PFOKM) and pseudo-second-order kinetic model (PSOKM) were used to fit kinetic cures of IMCFs and NIMCFs, equations are listed as follows (2), (3), respectively:

$$Q_t = Q_e - Q_e e^{-k_1 t} \tag{2}$$

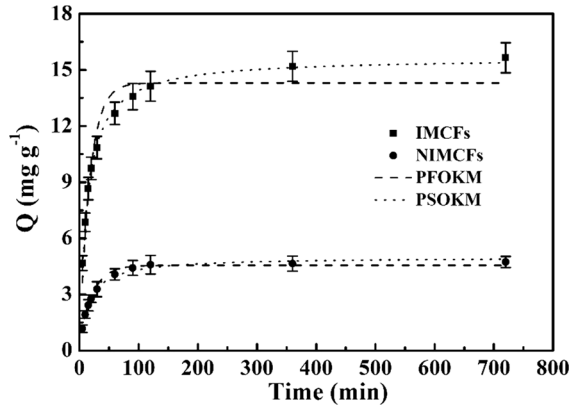

Fig. 3 Kinetic data and modelling for the adsorption of Gd(III) on IMCFs and NIMCFs, Error bar represents the standard deviation of kinetic data (pH = 7.0, 298 K, 50 mg L^{-1})

$$Q_t = \frac{k_2 Q_e^2 t}{1 + k_2 Q_e t} \tag{3}$$

where Q_t (mg g^{-1}) and Q_e (mg g^{-1}) are amounts of Gd(III) adsorbed per unit weight of sorbent at time t and equilibrium, respectively. k_1 (min^{-1}) and k_2 (g mg^{-1} min^{-1}) are rate constants of the PFOKM and PSOKM, respectively. The initial adsorption rate h (mg g^{-1} min^{-1}) and half equilibrium time $t_{1/2}$ (min) of the pseudo-second-order kinetic are also taken into discussion, according to Eqs. (4) and (5):

$$h = k_2 Q_e^2 \tag{4}$$

$$t_{1/2} = \frac{1}{k_2 Q_e} \tag{5}$$

The Gd(III) is adsorbed by imprinted sites on adsorbent surface within the first 50 min, accounts for about 80% of total adsorption process, then increased gently and eventually reached equilibrium in the next 5–6 h. Kinetic parameters calculated by PFOKM and PSOKM were summarized in Table 3. Compared with PFOKM, PSOKM fits the adsorption kinetics of IMCFs and NIMCFs better, with R^2 of 0.991 (IMCFs) and 0.997 (NIMCFs), respectively, which suggests adsorption mechanism is most likely the rate-limiting step. The h of IMCFs is higher than that of NIMCFs, while t of IMCFs is lower than that of NIMCFs. All results reveal that the existence of imprinted sites can prominently improve adsorption kinetic properties.

Table 3 Kinetic constants for the pseudo-first-order and pseudo-second-order models

Materials	$Q_{e,\ exp}$ (mg g^{-1})	Pseudo-first-order kinetic model			Pseudo-second-order kinetic model				
		$Q_{e,c}$ (mg g^{-1})	k_1 (min^{-1})	R^2	$Q_{e,c}$ (mg g^{-1})	$k_2 \times 10^2$ (g mg^{-1} min^{-1}) h (mg g^{-1} min^{-1})	$t_{1/2}$ (min)	R^2	
NIMCFs	4.734	4.558	0.0479	0.983	4.989	1.300	0.324	15.394	0.991
IMCFs	15.651	14.302	0.0587	0.936	15.640	0.509	1.246	12.560	0.997

Table 4 Thermodynamic parameters for Gd(III) adsorption

Materials	ΔH^o (kJ mol^{-1})	ΔS^o (J mol^{-1})	T (K)	K^o	ΔG^o (kJ mol^{-1})	R^2
IMCFs	1.44	19.95	298	7.37	− 4.95	0.999
			308	7.46	− 5.15	
			318	7.56	− 5.35	
NIMCFs	1.00	18.79	298	5.35	− 4.16	0.999
			308	5.45	− 4.34	
			318	5.55	− 4.53	

The effect of temperature

Thermodynamic tests were carried out under 298, 308, and 318 K. Owing to increased solution diffusion and decreased viscosity of solution, adsorption variates with temperature. Adsorption reflects the distribution of solute between liquid phase and interfacial adsorption phase. Adsorption equilibrium is denoted by $K°$, which is calculated by plotting ln (C_s C_e^{-1}) and C_s (Fig. S3). C_s is the amount of Gd(III) adsorbed per gram of the adsorbent at equilibrium (mmol g^{-1}), while C_e is the Gd(III) concentration in solution at equilibrium (mmol mL^{-1}). Standard free energy change is calculated by Gibb–Helmholtz formula Eq. (6). Values of enthalpy change ($\Delta H°$) and entropy change ($\Delta S°$) are calculated by the slope and intercept of the van't Hoff Eq. (7).

$$\Delta G^\circ = -RT \ln K^\circ \tag{6}$$

$$\ln K^\circ = \frac{\Delta S}{R} - \frac{\Delta H}{RT} \tag{7}$$

where R represents the symbol for universal gas constant (8.3145 J mol^{-1} K^{-1}) and T is the experimental temperature (K).

Table 4 summarizes thermodynamic parameters at different temperatures, values of gibb's free energy and enthalpy variation are also compiled. Positive values of enthalpy change ($\Delta H°$) and the decrease in Gibb's free energy change both indicate the adsorption reaction is endothermic. The effect of temperature changes on adsorption by IMCFs and NIMCFs and maximum adsorption equilibrium $K°$ at 318 K were shown in Fig. S4. All these results prove that the increase of temperature is beneficial to the adsorption process.

Adsorption isotherms

Adsorption isotherms are generally used to describe how adsorbates reach equilibrium between liquid and solid during adsorption. Langmuir and Freundlich isotherm models were used to analyze adsorption isotherm data in order to optimize experiment, which equations are expressed in Eq. (8) and (9), respectively. Fitted curves were depicted in Fig. 4, and corresponding parameters were listed in Table 5.

$$Q_e = \frac{K_L Q_m C_e}{1 + K_L C_e} \tag{8}$$

$$Q_e = K_F C_e^{1/n} \tag{9}$$

where K_L (L g^{-1}) and K_F (mg g^{-1}) are the affinity constant and adsorption capacity direction constant, respectively. $1/n$ indicates favorable adsorption conditions.

IMCFs display higher adsorption capacities than NIMCFs under same conditions, suggesting that

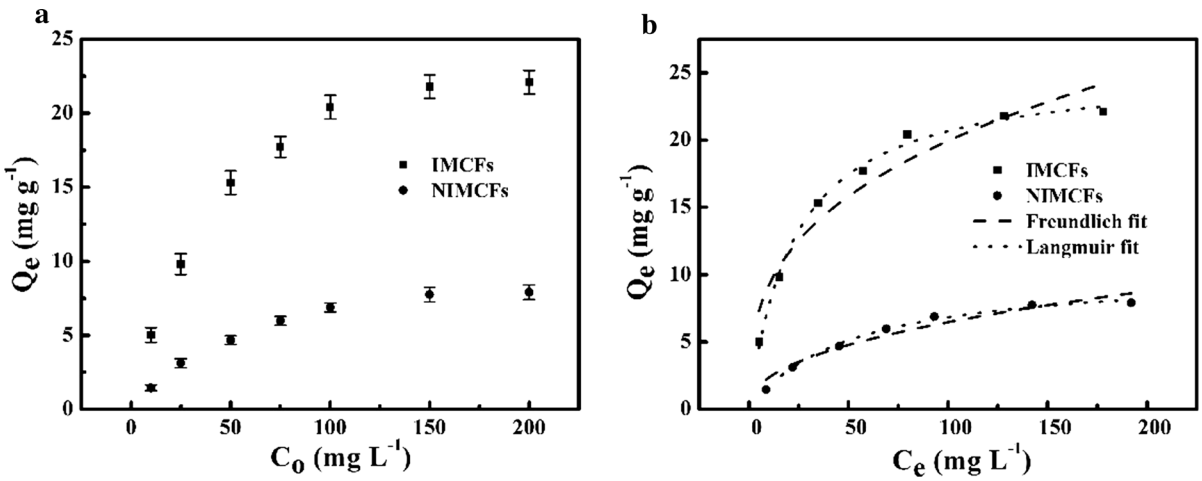

Fig. 4 Equilibrium data (**a**) and modelling (**b**) for the adsorption of Gd(III) on IMCFs and NIMCFs, Error bars represent the standard deviation of the kinetic data (pH = 7.0, 298 K)

Table 5 Adsorption equilibrium constants for Langmuir and Freundlich isotherm equations

Sorbents	Langmuir isotherm equation				Freundlich isotherm equation		
	R^2	K_L (L mg^{-1})	Q_m (mg g^{-1})	R_L	R^2	K_F (mg g^{-1})	1/n
NIMCFs	0.994	0.0198	10.293	0.2017	0.940	0.858	0.439
IMCFs	0.994	0.0440	25.372	0.1021	0.919	4.277	0.334

IMCFs show stronger affinity to Gd(III), this may due to the existence of imprinting sites in the IMCFs pore. In addition, imprinting materials provide a good spatial structure of carboxyl and amino coordination between Gd(III) and carboxymethyl chitosan, which make the adsorption of Gd(III) more favorable. The equation of Langmuir adsorption isotherm can better fit the experimental data of adsorption ($R^2 > 0.994$. Table 5). It presents a monolayer adsorption. The experimental saturated adsorption capacities of IMCFs and NIMCFs were 22.10 and 7.91 mg g^{-1} respectively, comparable with theoretical maximum adsorption capacities calculated by the Langmuir equation. Moreover, the separation factor or equilibrium parameter constant R_L, following the relationships as below Eq. (10):

$$R_L = \frac{1}{1 + C_m K_L} \tag{10}$$

where C_m is the maximum initial concentration of Gd(III).

R_L values of IMCFs and NIMCFs are 0.1021 and 0.2017, respectively, which are significantly smaller than those of NIMCFs and bulk imprinted films, which indicate imprinted films are more outstanding adsorbents for Gd(III).

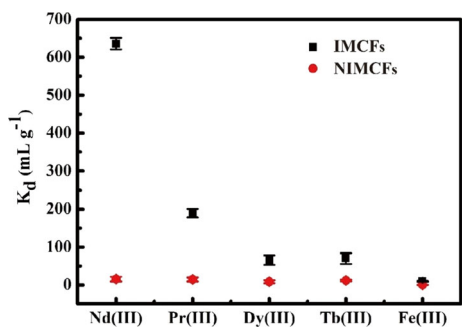

Fig. 5 K_d values of IMCFs and NIMCFs for a mixture of Nd(III), Pr(III), Dy(III), Tb(III), and Fe(III), error bars represent the standard derivation (pH = 7.0, 298 K, 50 mg L^{-1} for each ion)

Table 6 Comparison of REEs adsorption capacities for different sorbents

Sorbents	Cation	pH	Adsorption capacity (mg g^{-1})	References
3DIM-IFs	Gd(III)	7.0	51.36	Zheng et al. (2017)
Ionic imprinted resins based on EDTA and DTPA derivatives	Gd(III)	–	24.53	Vigneau et al. (2001)
Ionic imprinted chitosan/carbon nanotube composite	Gd(III)	7.0	88.00	Li et al. (2015)
Ion imprinted mesoporous silica	Dy(III)	2.0	17.45	Zheng et al. (2016a)
IMCFs	Gd(III)	7.0	25.37	This study

Selective adsorption tests

To investigate selective adsorption properties of IMCFs and NIMCFs, competition tests were performed in a coexisting system with four interfering cations (Dy(III), Nd(III), Pr(III), Tb(III) and Fe(III)). The concentration of each cation is 50 mg L^{-1}. The distribution coefficient (K_d, mL g^{-1}) is calculated by formula (11).

$$k_d = \frac{C_o - C_f}{C_f} \times \frac{V}{m} \tag{11}$$

where C_o and C_f are on the behalf of the initial and residual concentration of each cation.

Figure 5 shows that for Gd(III), the K_d value of IMCFs is obviously higher than that of NIMCFs. This may attribute to the coordination and imprinting of carboxyl groups on carboxymethyl chitosan. Based on Hard–Soft-Acid–Base Theory, carboxyl groups (–COOH) on the surface of IMCFs belong to hard base, while Gd(III) are traditional hard acid, then a great affinity occurs between them. But co-existing rare earth ions have similar chelating ability to carboxyl groups. Therefore, ion imprinting plays a critical role in the selective adsorption, which provides a specific imprinting site for Gd(III) and is inappropriate for another rare earth ions. Some other adsorbents are also summarized in Table 6 for comparison, and adsorption capacity varies with the change of adsorption conditions (Zheng et al. 2017; Vigneau et al. 2001; Li et al. 2015; Zheng et al. 2016a).

Reusability tests

Regeneration ability is one of the crucial factors in evaluating the value of adsorbents. The regeneration ability of IMCFs was evaluated by five cycles. As is shown in Fig. 6, the adsorption capacity of IMCFs is still 79% of the initial adsorption capacity after five cycles, the decrease may ascribe to the loss of active sites during the regeneration-binding process and/or incomplete desorption of Gd(III). The reusability tests fully prove that IMCFs, as an efficient, reliable and stable adsorbent, can be applied in the adsorption of REEs.

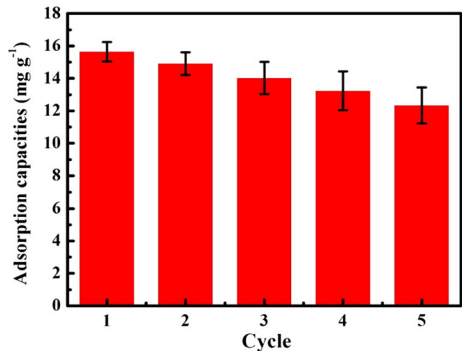

Fig. 6 Regeneration of IMCFs over five cycles. Error bars represent the standard error of the mean for measurements carried out in triplicate

Conclusions

In summary, free-standing imprinted mesoporous carboxymethyl chitosan films were fabricated for selective extraction of Gd(III) by a template-assisted assembly. Compared with general imprinted method, CNCs was used as bio-template, which is widely available, non-toxicity and has excellent chiral liquid crystal structure. Imprinted mesoporous carboxymethyl chitosan films greatly improve selective

adsorption and separation ability for Gd(III). Moreover, regeneration experiments show that the adsorbent has strong regeneration performance, which means great potential for industrial application.

Acknowledgments This work was financially supported by the National Natural Science Foundation of China (Nos. 21576120, 21446015, 21876015, 21808018, U1507115, and U1507118) and Natural Science Foundation of Jiangsu Province (Nos. BK20140534, BK20140580, BK20151350, and BK20131223).

References

Ayora C et al (2016) Recovery of rare earth elements and yttrium from passive-remediation systems of acid mine drainage. Environ Sci Technol 50:8255–8262

Bahrami A, Besharati-Seidani A, Abbaspour A, Shamsipur M (2015) A highly selective voltammetric sensor for nanomolar detection of mercury ions using a carbon ionic liquid paste electrode impregnated with novel ion imprinted polymeric nanobeads. Mater Sci Eng C 48:205–212

Cho A (2013) Hubs aim to reinvent DOE research culture. American Association for the Advancement of Science, Washington, pp 914–918

Dujardin E, Blaseby M, Mann S (2003) Synthesis of mesoporous silica by sol–gel mineralisation of cellulose nanorod nematic suspensions. J Mater Chem 13:696–699

Fu J, Chen L, Li J, Zhang Z (2015) Current status and challenges of ion imprinting. J Mater Chem A 3:13598–13627

Gao B, Zhang Y, Xu Y (2014) Study on recognition and separation of rare earth ions at picometer scale by using efficient ion-surface imprinted polymer materials. Hydrometallurgy 150:83–91

Guan M et al (2012) Assembling photoluminescent silicon nanocrystals into periodic mesoporous organosilica. J Am Chem Soc 134:8439–8446

He J, Chen JP (2014) A comprehensive review on biosorption of heavy metals by algal biomass: materials, performances, chemistry, and modeling simulation tools. Bioresour Technol 160:67–78

He J, Lu Y, Wu L, Luo G (2015) Continuous removal of lead from aqueous solutions by Ca(II) imprinted chitosan microspheres packed column. Sep Sci Technol 50:1127–1134

Kim D, Powell LE, Delmau LH, Peterson ES, Herchenroeder J, Bhave RR (2015) Selective extraction of rare earth elements from permanent magnet scraps with membrane solvent extraction. Environ Sci Technol 49:9452–9459

Kyzas GZ, Siafaka PI, Pavlidou EG, Chrissafis KJ, Bikiaris DN (2015) Synthesis and adsorption application of succinyl-grafted chitosan for the simultaneous removal of zinc and cationic dye from binary hazardous mixtures. Chem Eng J 259:438–448

Larsson K, Binnemans K (2014) Selective extraction of metals using ionic liquids for nickel metal hydride battery recycling. Green Chem 16:4595–4603

Li K et al (2015) Selective adsorption of Gd^{3+} on a magnetically retrievable imprinted chitosan/carbon nanotube composite with high capacity. ACS Appl Mater Int 7:21047–21055

Luo W et al (2016) A micelle fusion–aggregation assembly approach to mesoporous carbon materials with rich active sites for ultrasensitive ammonia sensing. J Am Chem Soc 138:12586–12595

Ma K, Sai H, Wiesner U (2012) Ultrasmall sub-10 nm near-infrared fluorescent mesoporous silica nanoparticles. J Am Chem Soc 134:13180–13183

Pavel CC, Thiel C, Degreif S, Blagoeva D, Buchert M, Schüler D, Tzimas E (2017) Role of substitution in mitigating the supply pressure of rare earths in electric road transport applications. Sustain Mater Technol 12:62–72

Qi H, Shopsowitz KE, Hamad WY, MacLachlan MJ (2011) Chiral nematic assemblies of silver nanoparticles in mesoporous silica thin films. J Am Chem Soc 133:3728–3731

Rollat A, Guyonnet D, Planchon M, Tuduri J (2016) Prospective analysis of the flows of certain rare earths in Europe at the 2020 horizon. Waste Manag 49:427–436

Shopsowitz KE, Hamad WY, MacLachlan MJ (2012) Flexible and iridescent chiral nematic mesoporous organosilica films. J Am Chem Soc 134:867–870

Smith YR, Bhattacharyya D, Willhard T, Misra M (2016) Adsorption of aqueous rare earth elements using carbon black derived from recycled tires. Chem Eng J 296:102–111

Thomas A, Antonietti M (2003) Silica nanocasting of simple cellulose derivatives: towards chiral pore systems with long-range order and chiral optical coatings. Adv Funct Mater 13:763–766

Vigneau O, Pinel C, Lemaire M (2001) Ionic imprinted resins based on EDTA and DTPA derivatives for lanthanides(III) separation. Anal Chim Acta 435:75–82

Wang L et al (2016) Loading actinides in multilayered structures for nuclear waste treatment: the first case study of uranium capture with vanadium carbide MXene. ACS Appl Mater Int 8:16396–16403

Woodcock P, Hayward MW (2016) Moving the goalposts: possible effects of changes in opportunity costs on conservation. Triage Front Ecol Evol 4:113

Xu J, Liu X, Lowry GV, Cao Z, Zhao H, Zhou JL, Xu X (2016) Dechlorination mechanism of 2,4-dichlorophenol by magnetic MWCNTs supported Pd/Fe nanohybrids: rapid adsorption, gradual dechlorination, and desorption of phenol. ACS Appl Mater Int 8:7333–7342

Yao W et al (2017) Enhanced removal of methyl orange on calcined glycerol-modified nanocrystallined Mg/Al layered double hydroxides. Chem Eng J 307:476–486

Zheng X, Wu D, Su T, Bao S, Liao C, Wang Q (2014) Magnetic nanocomposite hydrogel prepared by ZnO-initiated photopolymerization for La(III) adsorption. ACS Appl Mater Int 6:19840–19849

Zheng X, Liu E, Zhang F, Yan Y, Pan J (2016a) Efficient adsorption and separation of dysprosium from NdFeB magnets in an acidic system by ion imprinted mesoporous silica sealed in a dialysis bag. Green Chem 18:5031–5040

Zheng X, Pan J, Zhang F, Liu E, Shi W, Yan Y (2016b) Fabrication of free-standing bio-template mesoporous

hybrid film for high and selective phosphate removal. Chem Eng J 284:879–887

Zheng X, Zhang F, Liu E, Xu X, Yan Y (2016c) Efficient recovery of neodymium in acidic system by free-standing dual-template docking oriented ionic imprinted mesoporous films. ACS Appl Mater Int 9:730–739

Zheng X, Liu E, Zhang F, Dai J, Yan Y, Li C (2017) Selective adsorption and separation of gadolinium with three-dimensionally interconnected macroporous imprinted chitosan films. Cellulose 24:977–988